Linear Theory of Stratified Flow past an Isolated Mountain in Isosteric Coordinates

RONALD B. SMITH

Department of Geology and Geophysics, Yale University

(Manuscript received 21 March 1988, in final form 13 June 1988)

ABSTRACT

The linear theory for hydrostatic nonrotating flow over an axisymmetric hill is redone in isosteric (i.e., constant specific volume) coordinates, thus allowing the lower boundary condition (LBC) to be exactly satisfied. This results in a more consistent flow field near the mountain and good agreement with recent numerical calculations. The formation and spread of a region of collapsed density surfaces is predicted on the leeward slope. Two incipient stagnation points are predicted, one on the windward slope and one some distance aloft, above the mountaintop. In satisfying the LBC exactly, a correction to the pressure arises which cancels the Bernoulli "height term" in Sheppard's blocking analysis. This makes it seem unlikely that Sheppard's kinetic energy argument plays any role in airflow blocking and splitting.

1. Introduction

Recent study of the flow of a stratified fluid past an isolated hill has successfully described the far-field lee waves (Wurtele 1957; Crapper 1959; Palm 1958; Blumen 1965; Gjevik and Marthinsen 1977; Janowitz 1984), but has not answered the question of whether the low-level fluid trajectories will go around or over the hill for specified parameter values. Several approaches have been tried, but no complete answer has been found.

In the limit of steep sided obstacles and strong stratification, it has been shown by Drazin (1961) and Brighton (1978) that a power series expansion in small Froude number (U/Nh) gives the expected result that fluid parcels remain in horizontal planes as they move laterally around the hill. Further predictions by this approach are open to question as the expansion, carried to any order, does not capture gravity wave dynamics.

Laboratory experiments (Riley et al. 1976, Baines 1979; Hunt and Snyder 1980; Castro 1983; Snyder et al. 1985) have successfully illustrated the tendency for the low-level flow to go around rather than over the hill for Froude number less than about 1, but the reason for this behavior is still not clear.

Probably the best known conceptual model of the problem is that of Sheppard (1956), recently extended by Snyder et al. (1985). For an incompressible Boussinesq inviscid fluid with constant stability (N) and incoming speed (U), Bernoulli's equation on the surface can be written

$$u^2 = \frac{2}{\rho_0}\left[-p^* - \frac{1}{2}\rho_0 N^2 h^2\right] + U^2 \qquad (1)$$

where p^* is the deviation of the pressure at each point from the upstream pressure at the same height. Sheppard assumed $p^* = 0$ and thus concluded that a stagnation point ($u = 0$) should begin to form at the mountaintop $h = h_M$ when

$$\hat{h} = Nh_M/U \to 1.$$

The assumption $p^* = 0$ essentially reduces the problem to the question of whether the low level air, with its slightly higher density, has enough kinetic energy to climb the potential energy barrier of the mountain.

Another approach to the flow splitting problem is to linearize the hydrostatic equations of motion assuming small inverse Froude number (Smith 1980, henceforth S80; Phillips 1984). This method gives a solution for the hill induced velocity, density and pressure disturbance fields. For example, the axisymmetric hill of half-width a

$$h(x, y) = h_M/(1 + \hat{r}^2)^{3/2}; \quad \hat{r}^2 = (x/a)^2 + (y/a)^2 \qquad (2)$$

creates a pressure perturbation near the surface

$$p^*(x, y, z \approx 0) = -\rho_0 NUh_M(x/a)/(1 + \hat{r}^2)^{3/2}. \qquad (3)$$

Using (3) in (1) and neglecting the h^2 term for being of higher order

$$u^2 = 2NUh_M(x/a)/(1 + \hat{r}^2)^{3/2} + U^2 \qquad (4)$$

which predicts an incipient stagnation point on the centerline upstream of the mountain peak at ($x \approx -0.7$, $y = 0$, $z \approx 0$) when

$$\hat{h} \to 1.3.$$

Corresponding author address: Dr. Ronald B. Smith, Dept. of Geology and Geophysics, Yale University, Kline Geology Laboratory, P.O. Box 6666, New Haven, CT 06511-8130.

Thus while the critical values of $\hat{h}$ predicted by Sheppard and S80 are not so different, the underlying dynamics is completely distinct. Sheppard invokes the Bernoulli "height term" while S80 indicates that the flow is arrested by high pressure upstream of the hill associated hydrostatically with a positive density anomaly aloft.

The small amplitude assumption in S80 becomes increasingly questionable as $\hat{h}$ increases, because of both the linearization of the governing equations and the application of the lower boundary condition at $z = 0$ instead of $z = h$. The objective of this paper is to remove the latter approximation using isosteric coordinates. A secondary objective is to improve the analytic representation of the linear solutions to facilitate comparisons with laboratory and numerical experiments.

The final resolution of the splitting problem will probably be accomplished using a numerical model to find an exact solution to the nonlinear equations of motion (e.g. Thorsteinsson 1988, henceforth T88; Granberg 1983; Smolarkiewicz et al. 1988).

2. Linear theory in isosteric coordinates

Consider the set of equations governing inviscid, incompressible, hydrostatic fluid flow in isosteric coordinates (x, y, α)

$$D\mathbf{V}_H/Dt + \alpha\nabla_\alpha p + \nabla_\alpha\phi = 0 \tag{5}$$

$$D(\phi_\alpha)/Dt + \phi_\alpha\nabla_\alpha\cdot\mathbf{V}_H = 0 \tag{6}$$

$$\alpha\partial p/\partial\alpha + \partial\phi/\partial\alpha = 0 \tag{7}$$

where $\mathbf{V}_H = u\mathbf{i} + v\mathbf{j}$ is the horizontal velocity vector, p the pressure, $\phi = gz$ the geopotential, $\alpha = 1/\rho$ the specific volume and the total derivative operator

$$D(\ )/Dt = \frac{\partial(\ )}{\partial t} + \mathbf{V}_H\cdot\nabla_\alpha(\ ). \tag{8}$$

The subscript on the del operator indicates holding α constant while on a variable implies differentiation with respect to α. The set (5)–(7) is similar to that for isentropic flow in theta coordinates (Eliassen and Kleinschmidt 1957; T88), but the notation used here is an extension to three dimensions of an analysis by D. K. Lilly (personal communication, see also Granberg 1983). The compact form of (5)–(7) results from the constraint $D\alpha/Dt = 0$. Two conservation laws arise from (5)–(7),

$$\frac{D}{Dt}\nabla_\alpha\times\mathbf{V}_H = 0 \tag{9}$$

i.e., only vorticity vectors tangent to the α surfaces can be created by the pressure forces in (5). For steady flow, the Bernoulli equation is

$$\left[\frac{|\mathbf{V}_H|^2}{2} + \alpha p + \phi\right] = \text{constant on a streamline.} \tag{10}$$

If the lower surface at $z = h(x, y)$ coincides with an isostere (α_0), the lower boundary condition is

$$\phi(x, y, \alpha_0) = gh(x, y). \tag{11}$$

At large z, the radiation condition is applied. Linearizing (5)–(7) about a basic state $U(\alpha)$, $V(\alpha) = 0$, $\Phi_0(\alpha)$ gives

$$Uu'_x + \alpha p'_x + \phi'_x = 0 \tag{12}$$

$$Uv'_x + \alpha p'_y + \phi'_y = 0 \tag{13}$$

$$U\phi'_{\alpha x} + \Phi_{0\alpha}(u'_x + v'_y) = 0 \tag{14}$$

$$\alpha p'_\alpha + \phi'_\alpha = 0. \tag{15}$$

Assuming U and $\alpha\Phi_{0\alpha} = g^2/N^2$ are constant, (12)–(15) reduces to

$$\phi'_{\alpha\alpha xx} + \frac{g^2}{U^2N^2\alpha^2}(\phi'_{xx} + \phi'_{yy}) = 0. \tag{16}$$

Once ϕ' is found, the pressure can be recovered from

$$p'(x, y, \alpha) = -\int_\alpha^\infty \frac{1}{\alpha}\frac{\partial\phi'}{\partial\alpha}\,d\alpha. \tag{17}$$

Equation (16) can be rewritten in terms of an undisturbed height coordinate (z_0) and a vertical displacement (η), if we define $\alpha = \alpha(z_0)$ and $\eta = z - z_0$. Then with the Boussinesq approximation, (16) becomes

$$\eta_{xxz_0z_0} + \frac{N^2}{U^2}\nabla^2_{z_0}\eta = 0 \tag{18}$$

with

$$\eta(x, y, z_0 = 0) = h(x, y). \tag{19}$$

Akin to (17), the pressure perturbation can be expressed in terms of the perturbed thicknesses of isosteric layers.

$$p'(x, y, z_0) = g\int_{z_0}^\infty \frac{1}{\alpha(z_0)}\frac{\partial\eta}{\partial z_0}\,dz_0. \tag{20}$$

The solution to (2), (18), (19) from S80, is

$$\hat{\eta}(x, y, z_0) = \frac{1}{2\pi}\int\int_{-\infty}^\infty e^{-\hat{\kappa}}e^{i\hat{z}_0/\cos(\psi)}e^{i(\hat{k}\hat{x}+\hat{l}\hat{y})}\,d\hat{k}d\hat{l}, \tag{21}$$

where $\hat{x} = x/a$, $\hat{y} = y/a$, $\hat{k} = ka$, $\hat{l} = la$, $\hat{\kappa} = (\hat{k}^2 + \hat{l}^2)^{1/2}$, $\hat{z}_0 = z_0N/U$, $\psi = \tan^{-1}(\hat{l}/\hat{k})$, $\hat{\eta} = \eta/h_M$.

The height of each isosteric surface can be plotted from

$$z(x, y, z_0) = z_0 + \eta(x, y, z_0). \tag{22}$$

Note that the η-field from linear theory in geometric coordinates is often plotted in this same way, making

it appear that the lower boundary condition is satisfied when in fact it is not.

3. Representing the solution

Solution (21) is the three-dimensional analogue to the familiar two-dimensional hydrostatic mountain wave solution of Queney (1948). Unlike Queney's solution however, (21) cannot be simply expressed in terms of tabulated functions. Three methods are well-suited for determining the properties of (21): fast Fourier transform, asymptotic integral evaluation, and numerical contour integration.

a. Fast Fourier Transform

The integral in (21) can be quickly evaluated using a Fast Fourier Transform (FFT) algorithm. Slight errors arise from the periodic nature of the FFT and the ill-defined exponent in (21) when $\hat{k} = 0$. A typical solution is shown in Figs. 1 and 2.

b. Series expansion near $\hat{z}_0 = 0$

Following S80, (21) can be reduced to

$$\hat{\eta}(\hat{x}, \hat{y}, \hat{z}_0) = \frac{1}{2\pi}\int_0^{2\pi} \frac{e^{i\hat{z}_0/\cos(\psi)}d\psi}{(1 - i\hat{r}\cos(\psi - \theta))^2} \quad (23)$$

where $\theta = \tan^{-1}(\hat{y}/\hat{x})$.

Let

$$\hat{\eta}(\hat{x}, \hat{y}, \hat{z}_0) = a + b\hat{z}_0 + \frac{1}{2}c\hat{z}_0^2 + \cdots \quad (24)$$

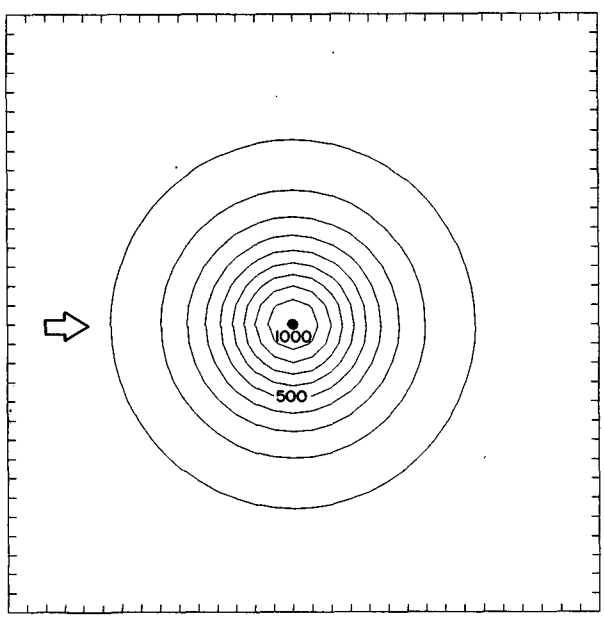

FIG. 1. The axisymmetric hill given by (2) with $h_M = 1000$. The contour interval is 100 and the hill half-width is five units.

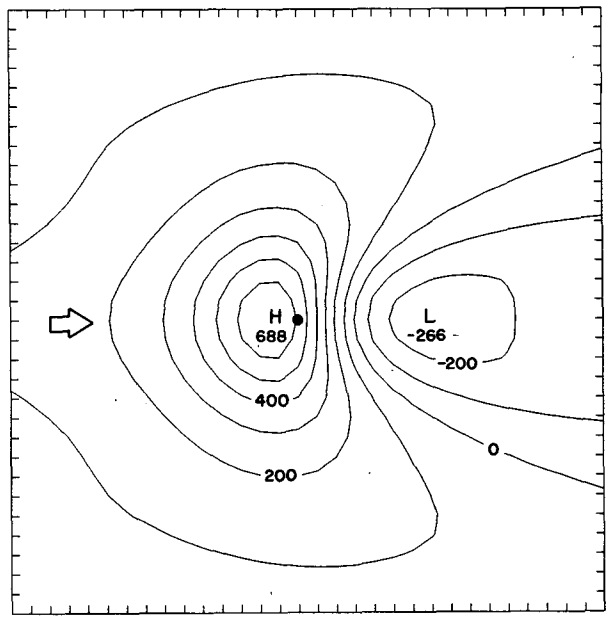

FIG. 2. The displacement of the $\hat{z}_0 = 0.5$ isosteric (or density) surface for the hill in Fig. 1, computed from (21) using a Fast Fourier Transform. The contour interval is 100 and the hilltop position is marked with a dot.

where each coefficient in (24) is evaluated from (23) at $\hat{z}_0 = 0$. Then

$$a = \hat{\eta}(\hat{x}, \hat{y}, 0) = F^{-3/2} \quad (25)$$

$$b = \hat{\eta}_{\hat{z}_0}(\hat{x}, \hat{y}, 0) = -\frac{1}{G}\left[1 - \frac{2\hat{y}}{G} + \frac{\hat{x}}{F^{3/2}} + \frac{\hat{x}(1 - \hat{y}^2)}{GF^{1/2}}\right] \quad (26)$$

$$c = \hat{\eta}_{\hat{z}_0\hat{z}_0}(\hat{x}, \hat{y}, 0) = \frac{3}{G}\left[-\frac{1}{3F^{3/2}} + \left(1 - \frac{4}{3G}\right)F^{-1/2} + \left(\frac{8}{3G^2} - \frac{2}{G}\right)(F^{1/2} + \hat{x})\right] \quad (27)$$

where $F = 1 + \hat{r}^2$ and $G = 1 + \hat{y}^2$. Expressions (26) and (27) are not Fourier integrable but can be derived from (23), nonetheless, by finding $\eta_{\hat{z}_0\hat{x}}$ and $\eta_{\hat{z}_0\hat{z}_0\hat{x}\hat{x}}$ respectively, and integrating them with respect to $\hat{x}$. The representation (24) is useful at all $\hat{x}$, $\hat{y}$ for $\hat{z}_0 < 0.5$ except in the wake $\hat{x} > 1$ and $|\hat{y}| < 1$ where the series converges poorly (see discussion in S80). An example of the use of (24) is given in Fig. 3.

The height of each low-lying constant density surface $z(x, y, z_0)$ can be plotted from (22), (24)–(27). If z_0 or η at a particular point (x, y, z) is desired, (22) and (24) can be solved. Keeping two terms in (24)

$$z_0 = \frac{z - a}{b + 1}. \quad (28)$$

Thus if $z = h$, $z_0 = 0$. If three terms are kept in (24), z_0 is found by solving

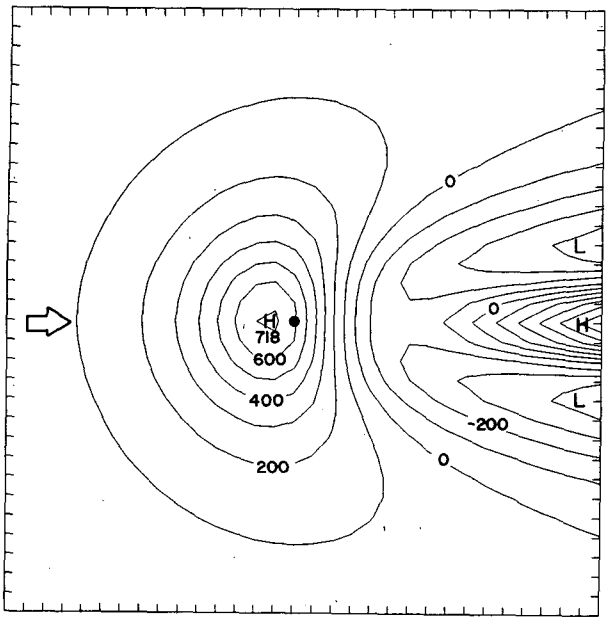

FIG. 3. As in Fig. 2, but computed from (24). Agreement with Fig. 2 is good except in the wake where the series (24) converges poorly.

$$\frac{1}{2}cz_0^2 + (b+1)z_0 + (a-z) = 0,$$

so

$$z_0 = \frac{-(b+1) \pm [(b+1)^2 - 2(a-z)c]^{1/2}}{c}. \quad (29)$$

At a point (x, y, z), only one root from (29) is physical.

c. Contour integration

Restricting to $\hat{y} = 0$ (i.e., $\theta = 0, \pi$), introducing a new variable

$$u = 1/\cos(\psi)$$

and using symmetry in the four quadrants of the integral, reduces (23) to

$$\hat{\eta}(\hat{x}, \hat{y} = 0, \hat{z}_0) = \frac{2}{\pi} \mathrm{Re} \int_1^\infty \frac{e^{i\hat{z}_0 u} du}{u\sqrt{u^2-1}(1 - i\hat{x}/u)^2}. \quad (30)$$

Only directly above the mountaintop at $\hat{x} = 0$ does (30) reduce to a known tabulated function. Taking $\partial/\partial\hat{z}_0$ of (30)

$$\hat{\eta}_{\hat{z}_0}(0, 0, \hat{z}_0) = \frac{2}{\pi} \mathrm{Re} \int_1^\infty \frac{e^{i\hat{z}_0 u} du}{\sqrt{1-u^2}}. \quad (31)$$

The contour integral in (31) is proportional to the First Hankel Function ($I = -(\pi/2)H_0^{(1)}(\hat{z}_0)$, Bowman 1958) whose real part is the Bessel Function of zero order. Thus

$$\hat{\eta}_{\hat{z}_0}(0, 0, \hat{z}_0) = -J_0(\hat{z}_0) \quad (32)$$

$$\hat{\eta}(0, 0, \hat{z}_0) = \left(1 - \int_0^{\hat{z}_0} J_0(\hat{z}_0) d\hat{z}_0\right) \quad (33)$$

$$\hat{\eta}_{\hat{z}_0\hat{z}_0}(0, 0, \hat{z}_0) = -\frac{d}{d\hat{z}_0} J_0(\hat{z}_0) = J_1(\hat{z}_0). \quad (34)$$

For $x \neq 0$, (30) can be numerically integrated (see Appendix). Streamlines in the $y = 0$ plane derived from (30) are shown in Figs. 4 and 5 for $\hat{h} = 0.5$ and 1.0, respectively.

4. Derived fields

To complete the theory, other dynamical fields must be determined. We restrict attention to fields which can be determined exactly from the $\eta(x, y, z)$ field described above. Thus if any error is present in the derived fields it is because of the linearization leading to (21) and not any subsequent linearizations. This will simplify later discussion.

a. Pressure

Two representations for the pressure field are considered: perturbation pressure on an α-surface (p') and on a level surface (p^*). In the Boussinesq limit [$\alpha = \alpha_0(1 + \gamma z_0)$; $\gamma z_0 \ll 1$] and with $N^2 = g\gamma = \text{const}$, the two are related by

$$p' = p^* - \rho_0 g\eta + \frac{1}{2}\rho_0 N^2 \eta^2. \quad (35)$$

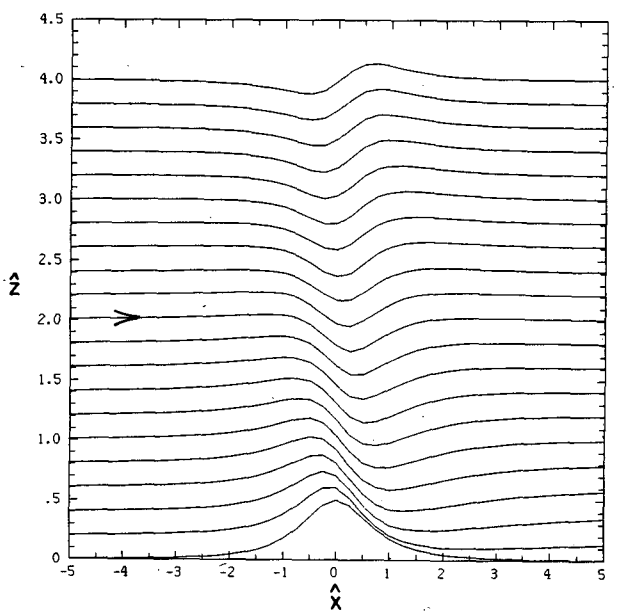

FIG. 4. Streamlines (or density surfaces) in the $y = 0$ plane for hill (2), computed from (30). The parameter $\hat{h} = 0.5$. Density surface collapse is beginning on the leeward slope.

Integrating (20) by parts with (22) gives

$$p' = -\rho_0 g\eta + \frac{1}{2}\rho_0 N^2\eta^2 + \rho_0 N^2 \int_z^\infty \eta dz', \quad (36)$$

so that from (35) and (36)

$$p^*(x, y, z) = \rho_0 N^2 \int_z^\infty \eta(x, y, z')dz' \quad (37)$$

as expected.

From (22)

$$dz = (1 + \eta_{z_0})dz_0 \quad (38)$$

and (37) becomes

$$p^*(x, y, z) = \rho_0 N^2\left[\int_{z_0}^\infty \eta(x, y, z_0')dz_0' + \int_\eta^0 \eta' d\eta'\right] \quad (39)$$

or

$$p^*(x, y, z) = \rho_0 N^2\left[\int_{z_0}^\infty \eta(x, y, z_0')dz_0' - \frac{1}{2}\eta^2\right]. \quad (40)$$

According to (40), two terms contribute to the pressure: a nonlocal term which arises from the integrated displacement field aloft, and a local term proportional to η^2 at the point of evaluation.

On the mountain surface $z_0 = 0$, $\eta = h$ so

$$p^*(x, y, z = h) = \rho_0 N^2\left[\int_0^\infty \eta(x, y, z_0)dz_0 - \frac{1}{2}h^2\right]. \quad (41)$$

The first term in (41) is the same as that arising in linear theory in z-coordinates (S80)

$$\rho_0 N^2 \int_0^\infty \eta(x, y, z_0)dz_0 = -\rho_0 NUh_M \frac{\hat{x}}{(1 + \hat{r}^2)^{3/2}}. \quad (42)$$

The second term in (41) describes a lowering of the surface pressure with respect to (42), arising from the use of isosteric coordinates to satisfy the lower boundary condition. Physically the correction is associated with the thinning of dense strata above the hill.

The pressure field on the hill surface [$p^*(z = h)$] can be used to compute the drag (D) on the hill according to

$$D = \int\int p^* \frac{\partial h}{\partial x} dxdy. \quad (43)$$

Using (2), (41) and (42), in (43), transforming to polar coordinates, and using a new variable of integration $(1 + r^2)$ gives

$$D = \frac{\pi}{4}\rho_0 aNUh_M^2. \quad (44)$$

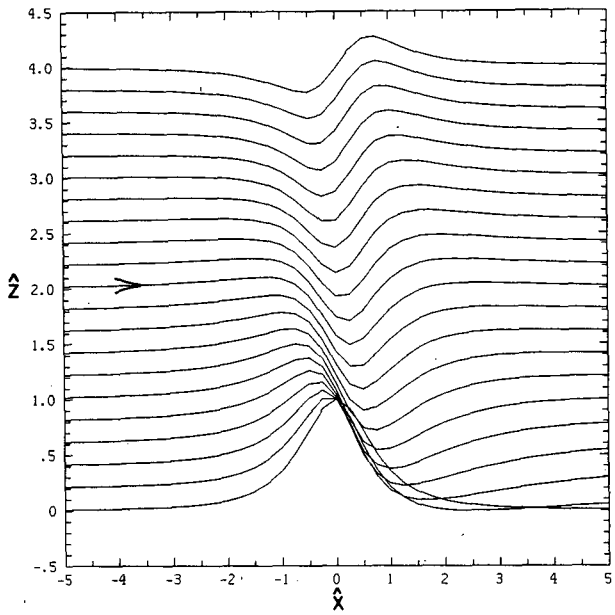

FIG. 5. As in Fig. 4, but with $\hat{h} = 1.0$. The penetration of density surfaces into the leeward hillside is unphysical and is caused by the linearization. Except for this penetration, the field of displacement agrees with T88 within 20%, for the same $\hat{h}$ value.

Note that the h^2 term in (41) is symmetric and makes no contribution to the drag. The result (44) could also be derived as a special case of the formulae given by Phillips (1984).

b. Wind speed

On any density surface $z = z_0 + \eta$ Bernoulli's equation (10) becomes

$$|\mathbf{V}_H|^2 = \frac{2}{\rho_0}\left[-p^* - \frac{1}{2}\rho_0 N^2\eta^2\right] + U^2 \quad (45)$$

where p^* is given by (40). At the lower boundary, as long as $\eta = h$, (41), (42) and (45) give

$$|\mathbf{V}_H|^2 = 2NUh_M \frac{\hat{x}}{(1 + \hat{r}^2)^{3/2}} + U^2. \quad (46)$$

The cancellation of the h^2 terms during substitution of (41) into (45) is important, as it eliminates the Bernoulli height term, the basis of the Sheppard energy argument. The cancellation arises as we apply Bernoulli's equation to a vertically displaced streamline on which the pressure is controlled hydrostatically by vertical displacements further aloft. Every time an α-surface slopes up, the parcels must lift against gravity, but lifting also thins the dense layers above and reduces the pressure slightly, which helps the parcels along.

Stagnation points aloft can be found from (40) and (45) by integrating (21) with respect to z_0 and evaluating the remaining double inverse transform with an FFT.

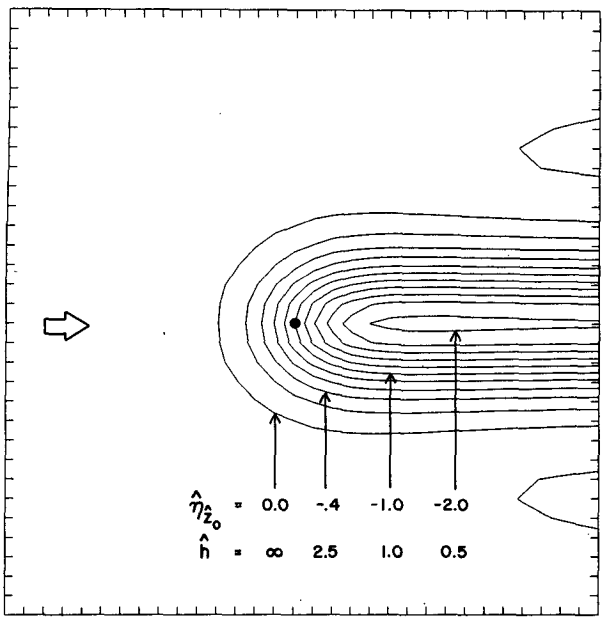

FIG. 6. The boundary of the collapsed density surface region as a function of $\hat{h}$, determined from $\eta_z = -1$ using (26).

5. Discussion

Two important features of the flow solution are the collapse of density surfaces on the leeward slope and the tendency for a stagnation point to develop on the windward slope and at a point aloft.

a. *The collapse of density surfaces*

The distance between two density surfaces separated upstream by Δz_0 is

$$\Delta z = \Delta z_0(1 + \eta_{z_0}) \tag{47}$$

and thus density surface collapse ($\Delta z \to 0$) occurs when $\eta_{z_0} \to -1$. From (26), this begins at the leeside point ($\hat{x} = 1$, $\hat{y} = 0$, $\hat{z}_0 = 0$) when $\hat{h} \approx \frac{1}{2}$. As $\hat{h}$ increases, the area of collapsed surfaces expands to cover more of the lee slope, bounded by a line on the hill surface where $\eta_{z_0} = -1$. The leading edge of the collapsed region reaches the hilltop when $\hat{h} = 1$ (26) or (32) and continues to advance for larger $\hat{h}$ (Fig. 6).

Inside the bounding line, the density surfaces given by (21) penetrate the hill surface slightly. This unphysical result is due to the linearization. An exact theory would either adjust the surfaces slightly upward in the collapsed region or indicate that no solution is possible with $z_0 = 0$ on $z = h(x, y)$. This second alternative is unlikely as it would require a stagnation point on the surface at the location of density surface collapse. The linear theory predicts no tendency for stagnation on the lee slope.

The collapsed region is associated with the horizontal divergence accompanying low level flow splitting. This tendency is so strong that even a particle starting higher than the hill peak could be brought down to nearly touch the lee slope. A few of the lower material surfaces remain collapsed some five to ten hill radii downstream.

b. *Incipient stagnation point*

According to (46), the air decelerates as it approaches the hill due to the increasing pressure. This deceleration increases with increasing $\hat{h}$ and at $\hat{h} \approx 1.3$, a stagnation point develops at the upstream point ($\hat{x} = -0.7$, $\hat{y} = 0$, $\hat{z}_0 = 0$). At this value of $\hat{h}$, the leading edge of the collapsed region is also upstream of the hill top at ($\hat{x} = -0.15$, $\hat{y} = 0$, $\hat{z}_0 = 0$). This proximity suggests that the leading edge of the collapsed zone will change its character from a point where isosteres begin to pack closely together without touching, to a point where a few of the lowest isosteres intersect the surface at a stagnation point. Parcels on the centerline of these isosteres split at the stagnation point and flow around the hill.

With the onset of stagnation, the hill surface no longer needs be an isostere. Thus, in addition to the doubtful quantitative validity of the linearization for $\hat{h} > 1$, the lower boundary condition (11) is no longer appropriate. The use of isosteric coordinates no longer simplifies the lower boundary condition.

The absence of a Sheppard height term in (46) seems to rule out the well-known kinetic energy argument for airflow blocking. The retardation associated with lifting dense fluid is exactly balanced by the hydrostatic decrease of pressure associated with thinning of dense layers aloft. This cancellation occurs at each point on the hill surface. It is true for any hill shape, not just (2). It is not restricted to the particular solution (21), but rather applies to any pattern of density surfaces which conforms to the hill and decays aloft. It would also apply to problems with vertical wind shear upstream, or problems with a Coriolis force or nonlinear terms included. It is restricted to incompressible inviscid hydrostatic flow with constant density on the hill surface (19), (37) and (43).

As $\hat{h}$ increases beyond $\hat{h} = 1$, a stagnation point also begins to form aloft at points near ($\hat{x} = 0$, $\hat{y} = 0$, $\hat{z}_0 = 4$) where $\eta = 0$. At such a point $u \ll U_0$ and the streamlines can be steeply sloping; a precursor to overturning. In 2-D flow, stagnation aloft occurs at significantly lower $\hat{h}$ than stagnation at the ground, but such is not the case here. The onset of stagnation aloft is retarded by the decay of 3-D wave field (i.e. $\eta \approx 1/\sqrt{z}$; see Appendix). The predicted critical value of $\hat{h}$, for stagnation aloft, is very close to that for surface stagnation $\hat{h}_{\text{crit}} = 1.3 \pm 0.1$. Given the errors in linear theory for such large $\hat{h}$, we cannot judge which stagnation point will form first. If the surface stagnation point forms first, it is possible that low level flow splitting could reduce the amplitude of the mountain waves so that stagnation aloft will never occur. If stagnation aloft occurs first, local overturning might occur which

could modify the flow field everywhere. In 2-D flow, the effect of stagnation aloft is profound (Clark and Peltier 1977).

6. Remarks

Consider the predictions of linear theory in isosteric coordinates, for flow over an axisymmetric hill.

$0 < \hat{h} < \frac{1}{2}$: Windward side deceleration, leeward side acceleration, weak streamline splitting, descent over hilltop and in the lee.

$\hat{h} = \frac{1}{2}$: Density surface collapse on the lee slope at $\hat{x} = 1$.

$\frac{1}{2} < \hat{h} < 1$: Region of collapsed density surfaces spreads to cover more of the lee slope. Upstream deceleration, downslope acceleration, and descent aloft become stronger. (Linear theory becomes quantitatively less accurate.)

$\hat{h} = 1$: Collapsed region reaches hilltop (good agreement with T88).

$1 < \hat{h}$: Collapsed region spreads onto the windward slope towards an incipient stagnation point. At some $\hat{h} = \hat{h}_{\text{crit}} \approx 1.3$, a stagnation point may form and isosteres intersect the hill surface. The center streamline splits. Overturning may occur aloft. (Linear theory not accurate.)

Comparison of these predictions with laboratory experiments is difficult, due to the use of steep models and modest Reynolds numbers in the experiments.

Comparison with the numerical experiments in T88 is possible if some account is taken of model differences. Thorsteinsson (1988) includes the Coriolis force but runs with Rossby number Ro = 4 minimize its effect. The artificial "divergence damping" in T88 may be important on the lee side where density surfaces are collapsing. Considering these differences, the linear theory streamline patterns in the $y = 0$ plane (Fig. 5) and the general shape and size of the lee side collapsed region (Fig. 6) compare well with T88's Figs. 8a and 8b for $\hat{h} = 1.0$. The use of θ-coordinates with a constant θ lower boundary, precludes the study of larger $\hat{h}$ values with pierced θ surfaces.

More recent numerical modeling in terrain following coordinates (Smolarkiewicz, personal communication 1988) indicates that windward side stagnation may begin when $\hat{h} \approx 1.8$, instead of the 1.3 value predicted here.

Although no suitable atmospheric datasets apparently exist, several locations would be acceptable for checking the current results: Cinder Cone Butte (Spangler 1987), Mt. Fuji, the Olympic Mountains, the mountains of Kauai, etc. Studies of airflow splitting around the Alps (Chen and Smith 1987) are on too large a scale to answer the questions posed here.

Acknowledgments. The unpublished notes on isosteric coordinates by D. K. Lilly were a stimulus for this work. The author is grateful for helpful discussions with D. Dempsey, P. Smolarkiewicz, S. Thorsteinsson, A. Eliassen, and the suggestions of an anonymous reviewer. This work was supported by the National Science Foundation Division of Atmospheric Sciences Grant ATM-8605939.

APPENDIX

Contour Integration

The convergence of integral (30) is improved if the contour is rotated to go from 1 to $1 + i\infty$. This does not change the value of the integral due to the analyticity of the integrand and the lack of a contribution from the large arc from ∞ to $i\infty$. This amounts to setting $u = 1 + iv$ and rewriting (30) as

$$\hat{\eta}(\hat{x}, 0, \hat{z}_0) = \frac{2}{\pi} \operatorname{Re}\left[ie^{i\hat{z}_0} \int_0^\infty \frac{(1 + iv)e^{-\hat{z}_0 v} dv}{\sqrt{v(2i - v)}(1 + iv - i\hat{x})^2} \right]. \quad (52)$$

The contribution to (52) from small v can be determined using a small step size or expressing the singular part of the integral as

$$I_\epsilon = \int_0^\epsilon \frac{(1 + iv)e^{-\hat{z}_0 v} dv}{\sqrt{v(2i - v)}(1 + iv - i\hat{x})^2} \approx \frac{1}{\sqrt{2i}} \frac{1}{(1 - i\hat{x})^2} [2\sqrt{\epsilon}]. \quad (53)$$

The remaining integral from ϵ to ∞ can be computed numerically using a trapezoidal rule. The optimum step size and upper limit of integration decrease as $\hat{z}_0$ increases.

Equation (52) is also convenient for asymptotic evaluation. For large $\hat{z}_0$ and $\hat{x} = 0$ the integral in (52) becomes (keeping two terms)

$$I \approx \left(\frac{1}{2i\hat{z}_0}\right)^{1/2} \left[\int_0^\infty \frac{e^{-\beta} d\beta}{\sqrt{\beta}} - \frac{5i}{4\hat{z}_0} \int_0^\infty e^{-\beta} \sqrt{\beta} d\beta \right]. \quad (54)$$

Then, with $\Gamma(1/2) = \sqrt{\pi}$ and $\Gamma(3/2) = 1/2\sqrt{\pi}$,

$$\hat{\eta}(0, 0, \hat{z}_0) \approx \left(\frac{2}{\pi\hat{z}_0}\right)^{1/2} [\cos(\hat{z}_0 + \pi/4) - (5/8\hat{z}_0) \cos(\hat{z}_0 + 3\pi/4)]. \quad (55)$$

This formula (55) agrees with (33) to within 10% for $\hat{z}_0 > 2$, 3% for $\hat{z}_0 > 5$, and 1% for $\hat{z}_0 > 8$.

REFERENCES

Baines, P. G., 1979: Observations of stratified flow past three-dimensional barriers. *J. Geophys. Res.*, **84**, 7834–7838.

Blumen, W., 1965: A random model of momentum flux by mountain waves. *Geofys. Publ.*, **26**, 1–33.

Bowman, F., 1958: *Introduction to Bessel Functions.* Dover, 135 pp.

Brighton, P. W. M., 1978: Strongly stratified flow past three-dimensional obstacles. *Quart. J. Roy. Meteor. Soc.*, **104**, 289–307.

Castro, I. P., 1983: Stratified flow over three-dimensional ridges. **135,** 261–282.

Chen, W.-D., and R. B. Smith, 1987: Blocking and deflection by the Alps. *Mon. Wea. Rev.,* **115,** 2578–2597.

Clark, T. L., and W. R. Peltier, 1977: On the evolution and stability of finite amplitude mountain waves. *J. Atmos. Sci.,* **34,** 1715–1730.

Crapper, G. D., 1959: A three-dimensional solution for waves in the lee of mountains. *J. Fluid Mech.,* **6,** 51–76.

Drazin, P. G., 1961: On the steady flow of a fluid of variable density past an obstacle. *Tellus,* **13,** 239–251.

Eliassen, A., and E. Kleinschmidt, 1957: Dynamic Meteorology. *Handbuch der Physik,* Vol. 48, J. Bartels, Ed., Springer-Verlag, 1–154.

Gjevik, B., and T. Marthinsen, 1977: Three-dimensional lee wave pattern. *Quart. J. Roy. Meteor. Soc.,* **104,** 947–957.

Granberg, I. G., 1983: Spatial problem of the flow of an incompressible stratified fluid over an obstacle (numerical modeling). *Izv., Atmos. Oceanic Phys.,* **19,** 267–272.

Hunt, J. C. R., and W. H. Snyder, 1980: Experiments on stably and neutrally stratified flow over a model three-dimensional hill. *J. Fluid Mech.,* **96,** 671–704.

Janowitz, G., 1984: Lee waves in three dimensional stratified fluid flow. *J. Fluid Mech.,* **148,** 97–108.

Palm, E., 1958: Two-dimensional and three-dimensional mountain waves. *Geofys. Publ.,* 20.

Phillips, D. S., 1984: Analytic surface pressure and drag for linear hydrostatic flow over three-dimensional elliptic mountains. *J. Atmos. Sci.,* **41,** 1073–1084.

Queney, P., 1948: The problem of airflow over mountains: A summary of theoretical studies. *Bull. Amer. Meteor. Soc.,* **29,** 16–26.

Riley, J. J., H.-T. Liu and E. W. Geller, 1976: A numerical and experimental study of stratified flow around complex terrain. Environmental Protection Agency Report EPA-60014-76-021.

Sheppard, P. A., 1956: Airflow over mountains. *Quart. J. Roy. Meteor. Soc.,* **82,** 528.

Smith, R. B., 1980: Linear theory of stratified hydrostatic flow past an isolated mountain. *Tellus,* **32,** 348–364.

Smolarkiewicz, P. K., R. M. Rasmussen and T. L. Clark, 1988: On the dynamics of Hawaiian Cloud Bands: Island Forcing. *J. Atmos. Sci.,* **45,** 1872–1905.

Snyder, W. H., R. S. Thompson, R. E. Eskridge, R. E. Lawson, I. P. Castro, J. T. Lee, J. C. R. Hunt and Y. Ogawa, 1985: The structure of strongly stratified flow over hills: Dividing streamline concept. *J. Fluid Mech.,* **152,** 249–288.

Spangler, T., 1987: Comparison of actual dividing streamline heights to height predictions using the Froude Number. *J. Climate Appl. Meteor.,* **26,** 204–207.

Thorsteinsson, S., 1988: Finite amplitude stratified airflow past isolated mountains on an f-plane. *Tellus,* **40A,** 220–236.

Wurtele, M., 1957: The three dimensional lee wave. *Beitr. Phys. frei. Atmos.,* **29,** 242–252.